Theoretical and experimental studies of chitin nanocrystals treated with ionic liquid or deep eutectic solvent to afford nanochitosan sheets

Catalina Ferreira Funes, Benjamin Bouvier, Christine Cézard, Claudia Fuentealba, Arash Jamali, Matthieu Courty, Caroline Hadad, Albert Nguyen van Nhien

Theoretical and Experimental studies of chitin nanocrystals treated with ionic liquid or deep eutectic solvent to afford nanochitosan sheets

Catalina Ferreira Funes,[a,b,c] Benjamin Bouvier,[a,b] Christine Cézard,[a,b] Claudia Fuentealba,[c] Arash Jamali,[e] Matthieu Courty,[d] Caroline Hadad,[a,b] and Albert Nguyen Van Nhien*[a,b]

[a] Laboratoire de Glycochimie, des Antimicrobiens et des Agroressources, UMR CNRS 7378, Université de Picardie Jules Verne - UFR des Sciences, 33 rue Saint Leu, 80039 Amiens Cedex, France.

[b] Institut de Chimie de Picardie FR CNRS 3085, 80039 Amiens, France.

[c] Pontificia Universidad Católica de Valparaíso, Escuela de Alimentos, Waddington 716, Playa Ancha, Valparaíso, Chile.

[d] Laboratoire de Réactivité et Chimie des Solides, UMR CNRS 7314, Université de Picardie Jules Verne, HUB de l'Energie, 33 rue Saint Leu - 80039 Amiens Cedex, France.

[e] Plateforme de Microscopie Electronique – Université de Picardie Jules Verne, HUB de l'Energie, 33 rue Saint Leu - 80039 Amiens Cedex, France.

*Email : albert.nguyen-van-nhien@u-picardie.fr

Abstract

Chitin nanocrystals have gained growing interest due to their many excellent properties, however the higher crystallinity of these nano-rod-shaped particles is a major hindering factor in preparation of nanochitosans with low degree of acetylation (DA). Here we studied the effect of the ionic liquid 1-ethyl-3-methylimidazolium acetate (IL) and deep eutectic solvent (choline chloride:lactic acid) (DES) pretreatments of chitin nanocrystals (NCChits) before the deacetylation step using both experimental and theoretical approaches. The results showed that the ionic liquid pretreatment was able to partially disrupt the crystalline structure leading to a lower DA (18.2%) after two cycles of deacetylation reaction. DES pretreatment, however, was unable to disturb the intra- and intermolecular hydrogen bonds, resulting in a DA of 73.6% similar to that of unpretreated chitin nanocrystals (73.2%). SEM images of chitin nanocrystals pretreated with ionic liquid showed that the crystals can rearrange into sheets. Molecular simulations reveal the detailed mechanism of chitin nanocrystal dissociation, in which the combination of a net molecular charge and hydrogen-bonding groups on a single scaffold (as is the case for [C_2mim] and [OAc]) plays a paramount role. These results can open the way to afford controlled nanochitosan sheets from chitin nanocrystals.

Graphical abstract

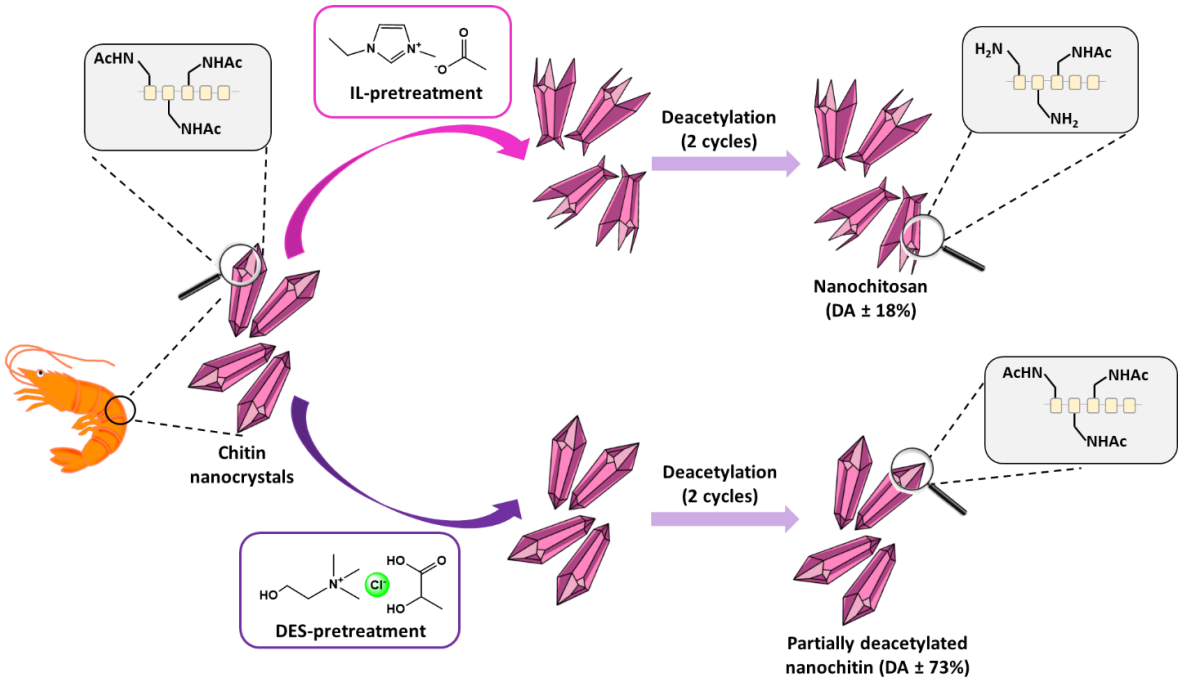

Highlights

(i) IL pretreatment was able to break partially the crystal leading to the formation of nanochitosan sheets.

(ii) DES-pretreatment was neither able to break the crystal nor to disturb the intra- and intermolecular hydrogen bonds.

(iii) Deacetylation reaction performed on IL-pretreated chitin nanocrystals was the strongest.

(iv) Combination of H-bonding capability and strong electrostatics in IL is mandatory for efficient chitin dissociation *in silico*.

Keyword: Chitin nanocrystals, ionic liquid, deep eutectic solvent, deacetylation reaction**,** molecular dynamics, intermolecular interactions.

1. Introduction

Chitin is a linear polysaccharide and the second most abundant natural polymer after cellulose on Earth. Chitin is an important constituent of the exoskeleton of crustaceans, algae, fungi and yeast and it is generally considered as an inexpensive, biocompatible, biodegradable and non-toxic material (Peniche et al. 2008, Ramos et al. 2016; González et al. 2018; González et al. 2014; Sun et al. 2020). Due to its many excellent properties, chitin perfectly meets up the demands with diversified

functionalities in applications and could be considered as a superior material for a sustainable future of industrial development. However, because of its insolubility in most organic and aqueous common solvents, chitin has long been considered an intractable polymer. Although much effort has been made over the past decade to overcome this issue, the lack of reproducibility of chitin solubility measurements still limits the development of products and access to the market in large volume (Roy et al. 2017). The source, molecular weight, batch-to-batch variability, strong hydrogen bond networks (inter- and intramolecular) and randomly distributed acetyl groups of chitin structure can be considered as factors resulting in problems of reproducibility (Deringer et al. 2016). Different types of solvents such as dichloroacetic acid (DCA), trichoroacetic acid (TCA) in presence or absence of alcohol (Austin 1975), dimethylacetamide (DMA)/LiCl mixture (Agboh and Qin 1997), $CaBr_2 \cdot H_2O$ saturated methanol (Wu et al. 2008), hexafluoroisopropyl alcohol and hexafluoracetone (Rinaudo 2006), lithium thiocyanate (Ma et al. 2011), phosphoric acid (Philippova et al. 2012) or *N*-methyl-2-pyrrolidone (Popa-Nita et al. 2010) have been used to solubilize chitin but many of these solvents are toxic, scarcely degradable, corrosive, or mutagenic. On the other hand, chitin can be converted into a more soluble compound namely chitosan with a lower degree of acetylation (DA < 50%) by removing the acetyl groups in C2 position under alkaline or enzymatic conditions. Chitosan that consists of randomly distributed β-(1-4)-linked *N*-acetyl-D-glucosamine (GlcNAc) and D-glucosamine (GlcN) shows superior properties including fluidity, water solubility and high water reducing ratio as well as some practical biological properties such as anticoagulant effects, controlled drug delivery, gelation, enhancement of permeation, mucoadhesion and antimicrobial properties (Hudson and Smith 1998; Jayakumar et al. 2007; Lv et al. 2014; Bravo-Osuna et al. 2007; Goy et al. 2009). The chemical conversion of chitin into chitosan, nevertheless, has several drawbacks such as the need for several consecutive reactions to reach low degree of deacetylation (DA), the production of abundant waste and a severe depolymerization occurring due to the strong alkaline reaction conditions (high concentration, time and temperature) (Goy et al. 2009; Wineinger et al. 2020; Lamarque et al. 2004).

New strategies, hence with better environmental and economic prospects have been developed, to overcome these limitations in the sustainable use of chitin. Recently, nanochitin has attracted the attention of researchers to take advantage of the structural characteristics of chitin at the nanoscale, including chitin nanocrystals (Bai et al. 2022), nanofibers (Jin et al. 2021b; Ifuku et al. 2013), nanodots (Devi and Dhamodharan 2018) or even nanoparticles (Guo et al. 2019). Nanochitin combines the advantages of neat chitin with the characteristics of nanomaterials, such as a high aspect ratio, high surface area, low density, rigidity, biocompatibility, low toxicity, antimicrobial activity, wound healing properties but also tunable photoluminescence properties (Feng et al. 2022; Bai et al. 2022; Jin et al. 2021b). Therefore, many applications have been described in the literature: food applications (Serventi et al. 2021), in biomedicine (Azuma et al. 2014) or for energy applications (Briscoe et al. 2015). Chitin

nanocrystals are defined as nano-rod-shaped structures that are highly crystalline (even more than 80% of crystallinity) and well-dispersed in water, spanning between 5–20 nm in width and hundreds of nm in length. Chitin nanocrystals correspond to the crystalline domains that can be isolated from chitin under certain specific conditions such as acidolysis (Tunjung Seta et al. 2021) or using deep eutectic solvent extraction (Hong et al. 2020). Conversion of nanochitin to nanochitosan, especially chitosan nanocrystals can increase its beneficial properties, however, this remains a challenging process due to the higher achieved degree of deacetylation (DA) and disruption of the crystalline structure (Pighinelli et al. 2016). Recently, the fabrication of carboxylated chitosan nanocrystals with high degree of deacetylation (DA < 20%) and narrow size distribution was described in the presence of $NaBH_4$ to preserve the nanorod structure of the biomaterial (Jin et al. 2020a). More recently, a novel chemical process to afford chitosan nanocrystals was described by Jin et al. (Jin et al. 2021a) by which a high degree of deacetylation, rod shape and high crystallinity for mechanical robustness could be achieved after 6 days of reaction. In a recent study, we compared the impact of both deep eutectic solvent (DES)- and ionic liquid (IL)-pretreatments on the efficiency of the chemical deacetylation of chitin (Huet et al. 2021). Chitin extraction and processing with DES and IL solvent are well documented in the literature (Li et al. 2022; Shamshina 2019). We also demonstrated that [C_2mim][OAc] IL and choline chloride (CC):lactic acid (LA)-DES impacted differently the chitin structure in terms of crystallinity: IL was a suitable solvent for chitin amorphization whereas DES preserved the α-chitin polymorphism and high crystallinity. Consequently, here we studied the impact of both [C_2mim][OAc]-IL and CC:LA-DES pretreatments directly on the crystalline structure of isolated chitin nanocrystals and their efficiency on the chemical deacetylation. The obtained nano-objects were characterized before and after pretreatment with the two different solvents and the efficiency of the deacetylation was measured using ^{13}C solid state NMR. Furthermore, molecular dynamics simulations provided atomic-resolution insights on the origin of the observed differences in the behavior of chitin nanocrystals in DES and [C_2mim][OAc].

2. Material and methods

2.1. Chemicals

All mineral acids and bases were used in their highest concentration commercially available from VWR Europe (Briaire, France) and Fischer Chemical (UK). Deionized ultrapure water (18.3 MΩ cm^{-1}) was obtained from Barnstead EASY pure RF water system (Iowa, USA) and used for all the experiments. 1-Ethyl-3-methylimidazolium acetate ([C_2mim][OAc], > 98%) was purchased from Proionic (Grambach, Austria). Choline chloride and lactic acid were supplied by Sigma-Aldrich (Streinheim, Germany).

2.2. DES synthesis

Choline chloride (CC) was mixed with lactic acid (LA) in a molar ratio of 1:2 in a glass bottle. The mixture was stirred for 24 h at 60 °C to homogenize the solution before use. After cooling DES was stored at room temperature.

2.3. Preparation of chitin nanocrystals using commercially available chitin from shrimp shells

Chitin from shrimp shells, supplied by Sigma–Aldrich (Steinheim, Germany), (4.0 g) was added to 80 mL of HCl (3 mol.L^{-1}) at 100 °C for 90 min and stirred under reflux. The pH was restored to neutral by centrifuging five times at 9500 rpm for 20 min with Milli-Q water (18.3 MΩ.cm^{-1}). The supernatant was removed at every centrifugation. The precipitate was then placed in MQ water and then into dialysis (dialysis sacks; Avg. flat width 35 mm (1.4 in), MWCO 12 000 Da) for three days. The water was replaced three times a day with fresh MQ water. The suspension was ultrasonicated for 10 min (1s on/1s off; 25% amp) (Vibra-cell 75022, 130 W, 20 kHz, sonic tip diameter 13 mm). The suspension was then centrifuged three times at 7500, 8500 and 9500 rpm and the precipitate was removed after each step. The final suspension contained the chitin nanocrystals (**NCChits**). Nanocrystals yield (33%) was determined by lyophilization of the final acquired suspension, and the concentration of chitin nanocrystals in colloidal suspension was estimated at 8.95 g.L^{-1}. The **NCChit** dispersion was stored in a refrigerator to prevent bacterial growth.

2.4. DES- and IL-pretreatment of chitin nanocrystals

Dried chitin nanocrystals were weighed and 1.5 g of the powder was introduced into 50 mL of DES or IL (3% w/v) at 80 °C for 24 h under stirring. The reaction was stopped by adding 130 mL of MQ water, and then the mixture was centrifuged five times. Subsequently, dialysis was performed for 3 days to remove any rest of DES or IL. Samples were lyophilized to determine the yields of chitin nanocrystals resulting from DES or IL pretreatments. The calculated yields were 65.3% for DES and 78.6% for IL, thereafter named **DES-pretreated NCChits** and **IL-pretreated NCChits** respectively.

2.5. Deacetylation reaction

Untreated and pretreated chitin nanocrystals were deacetylated following the methodology of Jin *et al*., (Jin et al. 2020b) with slight modifications. In a typical experiment, 500 mg of untreated **NCChit**, **IL-** or **DES-pretreated NCChits** were added to 50 mL of a solution of NaOH (40% w/w) with addition of sodium borohydride (10% w/w). The mixture was heated overnight (18 h) at 117 °C under stirring. After this first cycle of deacetylation, the suspension was centrifuged at 9500 rpm for 10 min, the supernatant was removed, and the pellet was resuspended in fresh NaOH and heated overnight as described above for the first cycle. The resulting suspension was recentrifuged under the same

condition as cycle one, and the recovered solid was washed with MQ water by several centrifugation cycles (9500 rpm, 10 min) until pH = 8. Then, the resulting chitosan and partially deacetylated chitins were resuspended in MQ water and HCl (1 M) was added until pH ± 5 and finally, the suspension was lyophilized. Yields of **untreated partially deacetylated NCChits**, **DES-partially deacetylated NCChits and IL- NCChitosan** after two cycles are summarized in Table 1.

2.6. Solubility tests

The solubility of the synthesized **untreated partially deacetylated NCChits**, **DES-partially deacetylated NCChits, IL-NCChitosan** and that of commercially available low molecular weight chitosan (LMW, 50,000-190,000 Da (based on viscosity)) were measured and compared by their solubilization in MQ water and 1% acetic acid aqueous solution at a concentration of 10 $mg.mL^{-1}$.

2.7. Instrumental analysis

CP-MAS ^{13}C NMR spectra were obtained at 125 MHz using a Bruker AVANCE III HD spectrometer 500 MHz. The pulse sequence was based on cross-polarization techniques. The rotation frequency of samples was 15 kHz and the contact time was optimized to 2 ms with a 5 s delay between scans to observe correctly all the carbons of chitin nanocrystals derivatives. The probe used allowed the use of a 2.5 mm rotor. Degrees of acetylation (DA) were determined by integration of the *N*-acetyl carbon atom divided by the sum of the intensities of the D-glucopyranosyl carbon ring atoms. Deacetylation treatment refers to the process of removal of acetyl groups from chitin nanocrystals, and acetylation degree determines the content of remaining *N*-acetyl groups. X-Ray powder diffraction (XRD) patterns were acquired using a Bruker D8 Endeavor diffractometer equipped with a Cu anti-cathode (Kα radiation, operating at 40 kV–40 mA). Patterns were collected in the 2θ range of 10–60° with a step size of 0.03° and using a low background silicon holder (Bruker AXS, C79298A3244B261). The experimental conditions used for the measurement did not allow us to correctly observe the band below 10°. The crystallinity index (CrI) was estimated using an empirical equation described by Fan et al. (Fan et al. 2008a): $CrI = ((Intensity_{110}-Intensity_{amorph})/Intensity_{110})*100)$, where I_{110} is the intensity of the main peak (110) and I_{amorph} is the intensity of the amorphous portion at 2θ = 16.0°. Scanning electron microscopy (SEM) was used to examine the microstructure of chitin, untreated and IL/DES-pretreated chitin nanocrystals, and the resulting nanochitosans. A small amount of dried samples (powder or flakes) was placed on double-sided carbon tape adhered to aluminum SEM stubs. These were then coated with a 20 nm layer of gold and examined using a Quanta 200 FEG scanning electron microscope (FEI Co., USA). The micrographs were obtained with a secondary electron detector at an accelerating voltage of 2 or 5 kV. Transmission electron microscopy (TEM) images were acquired with a Tecnai G2 f20 S-Twin electron microscope (FEI, Eindhoven, the Netherlands) operating at 200 kV.

Sample were prepared at a concentration of 0.1 mg.mL^{-1} in MQ water. The suspension was sonicated for 5 minutes and a 5 µL droplet was placed onto a 300 mesh copper TEM grid, dried and stored for observation. Infrared spectra were obtained using a Fourier-transform infrared (FT-IR) spectrometer (IRaffinity-1S, Shimadzu) and ATR method with a germanium prism (MIRacle 10, Shimadzu). Spectra were obtained in a range between 700 cm^{-1} and 4000 cm^{-1} at a resolution of 4 cm^{-1} with 64 scans. Thermogravimetric analysis (TGA) was recorded on a Netzsch STA 449C Jupiter thermal analyzer instrument equipped with a differential analysis microbalance coupled to a QMS 403 Aëolos mass spectrometer with a stainless-steel capillary and a Secondary Electron Multiplier (SEV) detector (Channeltron). The counting time for the mass spectrometer was 20 ms per (m/z) value (scanning width: m/z = 10–150 amu) with a resting time of 1 s. The samples (approximately 20 mg of each compound) were heated in an alumina crucible under argon, by equilibrating at 25 °C, and followed a ramp at 5 °C.min^{-1} up to 800 °C and an isotherm under air atmosphere for 30 min (Flow rate: 50 mL.min^{-1}). Zeta potential was evaluated with a Zetasizer Nano PRO (Malvern Instruments) working with a 633 nm laser and at two scattering angles of 173 and 13°, respectively. Samples were allowed to equilibrate at 25°C for 120 s before measurement to avoid artifacts from convection. Zeta potential evaluation was performed in single-use disposable folded capillary cells commercialized by Malvern Instruments (model DTS 1070). All sample were prepared at a concentration of 1 mg.mL^{-1} in MQ water.

2.8. *In silico* simulations

The starting structure for the 9-chain × 10-mer chitin model was constructed using experimental crystallographic data taken from reference (Sikorski et al. 2009). It was described using the GLYCAM06 force field (Kirschner et al. 2008). The force field parameters for the molecules composing the [C_2mim][OAc] and DES solvents were developed based on the GAFF force field (Wang et al. 2004) except for water whose parameters were taken from the TIP3P model (Jorgensen et al. 1983). For the [C_2mim][OAc] ionic liquid, the atomic charge scaling factor was set to 80% as per previous studies (Uto et al. 2018).

Solvent boxes containing [C_2mim][OAc] on the one hand, and a mixture of lactic acid, choline chloride and water on the other, were generated according to experimental composition ratios. Lactic acid molecules consisted of 50% R and 50% S chiralities. The boxes were equilibrated at 300 K for 50 ns under a pressure of 1 bar.

Chitin crystals (9-chain × 10-mer) were introduced in truncated octahedral boxes containing each of the two solvents. The systems were minimized, simulated with restraints on the chitin heavy atoms for 10 ns at constant volume and a temperature of 300 K, then for 10 ns at a constant 1 bar pressure. This system was duplicated and its temperature was ramped to 450 K in 10 ns. The restraints were removed

and preproduction simulations were run for 20 ns in the NPT ensemble at both temperatures. Production runs of 500 ns were then performed under similar conditions. The temperature and pressure were respectively regulated using the velocity-rescaling (τ = 2 ps) and Parrinello-Rahman (τ = 5 ps, compressibility = 4.5 10^{-5} bar^{-1}) algorithms. The equations of motions were integrated using a 2 fs time step. Periodic boundary conditions were imposed in all dimensions of space. Short-range Coulomb and van der Waals forces were cut off at 1 nm, while long-range electrostatics were computed with the particle-mesh Ewald method. All simulations were performed and analyzed using the CUDA-enabled version of the GROMACS 2021.4 suite (Abraham et al. 2015). The value of 450 K was chosen as an *in silico* counterpart to the experimental dissociation temperature of 353 K (80 °C) for two reasons: (i) Because of the lack of entropic terms and explicit temperature dependence in the GLYCAM and GAFF force fields (which are parameterized at 300 K), the temperature-dependent weakening of attractive interactions is generally insufficient, resulting in simulated molecular systems that are too stable compared to experiments performed at the same temperature for temperatures above 350 K. (ii) The experimental DES and IL pretreatments of chitin nanocrystals were carried out over 24 hours, a timespan which is orders of magnitude too long for molecular dynamics simulations on state-of-the-art computer hardware. Indeed, previous reports have shown that temperatures of 400 K or lower are insufficient to dissolve chitin crystals within tractable simulation timescales (Uto et al. 2018). By using higher simulated temperatures, the chitin dissolution process can be readily accelerated to within amenable durations, with limited impact on the underlying mechanism.

3. Results and discussions

3.1. Synthesis and characterization of chitin nanocrystals

We used acid hydrolysis to obtain chitin nanocrystals from commercially available chitin. Chitin was hydrolyzed with an aqueous hydrochloric acid solution (3 M HCl) for 1.5 h at 90 °C, quenched with water, followed by several steps of centrifugation and dialysis to reach neutral pH. Acid hydrolysis, as proposed in more recent protocols, is used to destroy the amorphous regions of chitin and leave the highly crystalline regions almost intact (Goodrich and Winter 2007a). The selected reaction time and temperature used here, prevented undesirable results such as the decrease in crystallinity induced by destruction of crystalline parts as reported previously (Goodrich and Winter 2007a). Further steps in chitin nanocrystal preparation included ultrasonication to improve dispersibility and centrifugation to remove aggregates. The resulting dispersion had a white/beige color and a concentration of 8.95 $mg.mL^{-1}$ that could remain stable over a period of months. Furthermore, the lyophilization of the acquired dispersion could prevent bacterial contamination and the following characterization of the resulting **NCChits.**

The FTIR spectra of the commercial chitin revealed the α-chitin organization by featuring two characteristic peaks at around 1660 cm^{-1} and 1620 cm^{-1} of the C-O bonding of the amide function (see ESI, Figure S1-A). Similarly, the FTIR spectra of **NCChits** (Figure S1-A) showed well-defined peaks at 1658 cm^{-1} and 1621 cm^{-1} corresponding to the amide I region and an absorbance peak at 1560 cm^{-1} corresponding to the amide II. These spectral features could confirm that the α-structure was preserved during the hydrolysis process. Furthermore, the crystallographic α-structure has also been confirmed by solid state ^{13}C NMR. The spectra revealed the presence of C_3 and C_5 signals characteristic of the α type-chitin at around 75 and 73 ppm (see ESI, Figures S2 and S3). Amongst several spectroscopic and analytical methods that have been developed to determine the degree of acetylation (DA) in chitin/chitosan, the solid state ^{13}C NMR is one of the most accurate approaches. Using this method, the DA was calculated by measuring the integral of the methyl group at around 23 ppm divided by the integral of all the carbon atoms in the backbone. The DA from CP-MAS NMR was calculated to be 100% for the chitin nanocrystals and 87% for the commercial chitin, indicating that the hydrolysis treatment removed amorphous domains containing glucosamine units. The crystallinity indexes (CrI) of the **NCChits** and the commercial chitin were calculated on the basis of X-ray diffractograms shown on Figure S1-B, using the intensity method (see formula in the experimental part). As shown in Figure S1-B, diffractogram of the commercially available chitin indicated the typical characteristics of α–chitin with the diffraction peaks at 2θ of 12.7, 19.3, 23.1 and 26.6° corresponding to 020, 021, 110, 120 and 130 planes, respectively. The same behavior was observed for the chitin nanocrystals with the diffraction peaks at 2θ of 12.7, 19.2, 23.2 and 26.6°. A significant increase of the crystallinity index of chitin nanocrystals could be noted compared to the commercial chitin confirming the removal of the amorphous regions, 75% *versus* 93% (Table 1).

SEM images of commercial chitin and **NCChits** are represented in Figure S4 (see ESI). The SEM observation of commercial chitin and **NCChits** showed the significant differences as expected in their morphology and particle size. The commercial chitin samples contained large particles ranging from several tens to several hundreds of micrometers while nanosized objects were observed in the **NCChits** samples (Figure S4-ESI). Transmission electron microscopy (TEM) of **NCChits** confirmed the structural transformation of commercial chitin as a result of acid hydrolysis and the formation of nanosized needles (Figure 1-A). The acquired images were also used to measure the size of the resulting nanosized needles in **NCChits.** The length distribution of 153 $\pm$ 60 nm was determined by measuring single and clear nanoparticles in the TEM images (Figure 1-B).

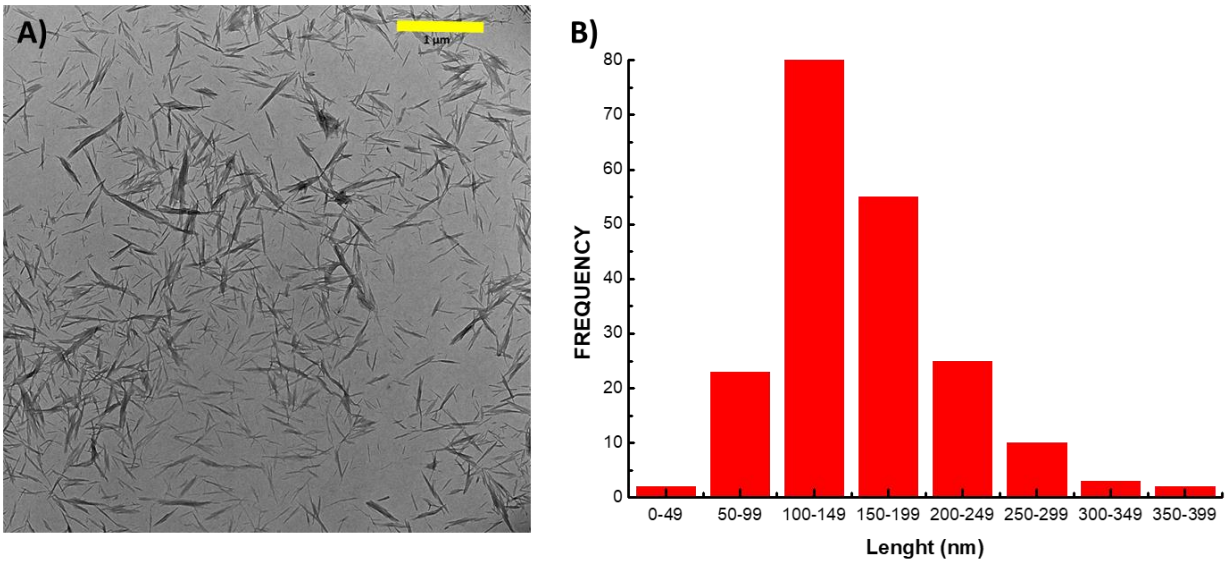

Figure 1. A TEM image of the NCChits (A) and the length distribution of the NCChits (B). Scale bar = 1 µm.

3.2. Impact of IL- and DES-pretreatment of chitin nanocrystals on the deacetylation efficiency

Acidic and basic ionic liquids have been intensively studied on chitin. In the first case, the less acidic phosphonate anion has shown no impact on chitin following the Kamlet-Taft parameters (Husson et al. 2017) whereas an IL containing [HSO_4]- anions has demonstrated its ability to extract cellulose or chitin nanocrystals (Mincea et al. 2012; Shamsuri et al. 2022; Douard et al. 2021). Basic IL are able to disrupt chitin but their basicity is not strong enough to modify the chitin chemical structure (no deacetylation process). In a similar trend, acid/basic based deep eutectic solvents have proved their ability to extract, solubilize cellulose or chitin or to isolate nanocrystals (Özel and Elibol 2021; Sharma et al. 2013; Li et al. 2022) . We chose a DES made of choline chloride:lactic acid (CC:LA) which had been described as the most efficient in terms of chitin solubilization. Indeed, in a study described by Wang et al. (Wang et al. 2021), several DES such as choline chloride/lactic acid (CC:LA), choline chloride/malic acid (CC:MA), choline chloride/propanoic acid (CC:PA), choline chloride/urea (CC:U), choline chloride/glycerol (CC:G), betaine/lactic acid (B:LA), betaine/glycerol (B:G) or betaine/propanoic acid (B:PA) were tested. The acidic DES CC:LA gave the best results followed by the basic DES CC:U. In the work described by Vicente et al. (Vicente et al. 2020), the DES CC:LA and CC:U were both used to solubilize chitin and then the deacetylation reaction of chitin was performed under classical conditions. However, the obtained results showed that the use of DES CC:U was not possible for the deacetylation of chitin into chitosan since a secondary reaction could take place between the residual urea and NaOH, leading to the formation of a brown solid with the release of ammonia and CO_2. Another study (Bisht et al. 2021) also showed that the use of CC:LA DES with a 1:2 ratio was one of the most effective for chitin solubilization and no deacetylation occured with this DES (Hong et al. 2018). Therefore, basic

1-ethyl-3-methylimidazolium acetate [C_2mim][OAc] and DES made of choline chloride and lactic acid in a 1:2 ratio were used to pretreat the chitin nanocrystals for 24 h at 80 °C and their impact on the crystallinity, size, morphology and chemical properties was studied.

The FTIR spectra showed that the α-pattern in **NCChits** disappeared as a result of IL-pretreatment of **NCChits** (Figure 2A). This is in accord with our previous studies showing that a [C_2min][OAc] pretreatment partially solubilized chitin, breaking hydrogen bonds and disrupting its supramolecular structure (Huet et al. 2021; Huet et al. 2020a; Huet et al. 2020b). DES pretreatment, however, did not have the same effects since the two characteristic peaks of the amide C-O bonding were still present in the spectra (Figure 2-A). These results are fully in line with those obtained by XRD where the α-structure was maintained for **DES-pretreated NCChits** in contrast to **IL-pretreated NCChits**. The results of crystallinity index measurements showed that DES-pretreatment on **NCChits** induced no significant decrease in the CrI (93% *vs* 91%) while IL-pretreatment induced a significant decrease (93% *vs* 79%) in crystallinity (Table 1). These values are similar to the ones described in the literature with chitin nanocrystals (Gueye et al. 2016). The impact of both pretreatments could also be confirmed by thermogravimetric analysis (Table 1 and see also ESI, Figure S5). The first mass loss (< 10 %) observed below 100 °C for all samples corresponds to the water loss and the second one took place at around 270 °C as a result of the decomposition of *N*-acetamido groups. By comparing the DTG_{max} (Table 1) ascribed to the decomposition of the backbone of the commercially available chitin (Yuan et al. 2020) and the one of the **untreated NCChits** and **DES-pretreated NCChits**, 378 °C, 384 °C and 380°C respectively, we could conclude that there was no significant thermal stability difference between chitin and nanocrystals. However, after IL-pretreatment, a slight decrease can be observed (DTG_{max} = 352 °C). The slight thermal variation could be explained by the hydrogen bond breakings at the edge of the polymer caused by the penetration of [OAc] from IL. It was shown that the effect of the ionic liquid pretreatment on the thermal stability was much more pronounced than that using DES pretreatment (Zhong et al. 2020). However, here we observed a decrease in the total mass of recovery of pretreated **NCChits**, by 34.7% in the case of DES pretreatment and by 21.4% in the case of IL (Table 1). The higher loss for DES-pretreatment compared to IL-pretreatment could be explained by acidic hydrolysis of the amorphous region.

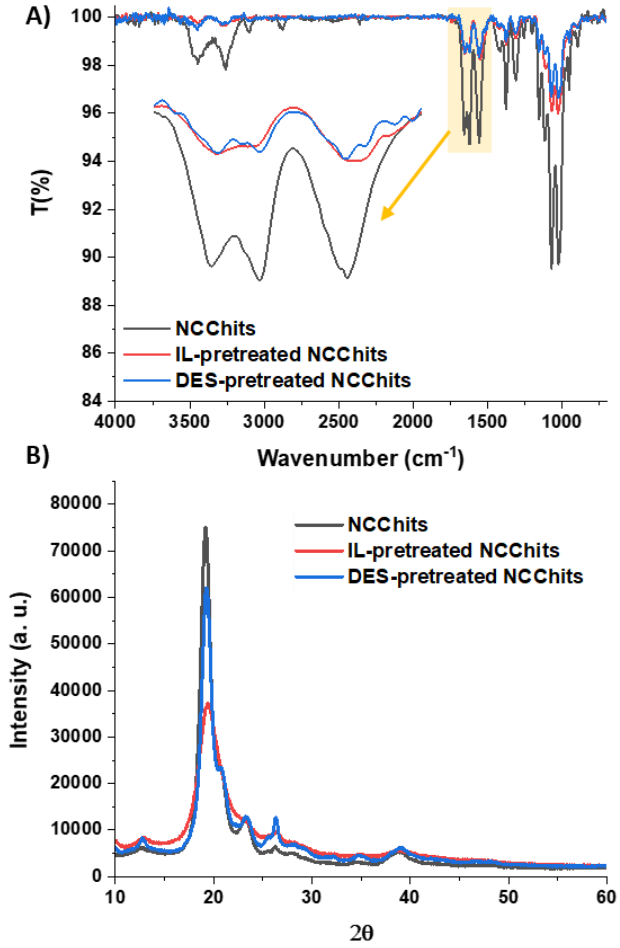

Figure 2. A) ATR-FTIR spectra of NCChits (black line), IL-pretreated NCChits (red line) and DES-pretreated NCChits (blue line). Inset: Zoom of the 1700-1500 cm^{-1} range. B) XRD of NCChits (black line), IL-pretreated NCChits (red line) and DES-pretreated NCChits (blue line).

Deacetylation reactions were then performed on **NCChits**, **IL-** and **DES-pretreated NCChits**. It is noteworthy to point out that the reaction effectiveness is strongly dependent on the polymer crystallinity and without a specific procedure, a highly crystalline chitin leads preferentially to a low deacetylation degree localized at the surface (Pereira et al. 2014; Dhillon et al. 2013). The first deacetylation reaction of chitin nanocrystals was reported by Chirachanchi et al. (Phongying et al. 2007). A concentrated aqueous solution of NaOH (40% w/w) at high temperature (100 to 180 °C) for a long period of time led to DA of 2% but resulted in drastic changes in the crystallinity and morphology. A lower temperature has been then used under basic media where nanocrystals with DA at a maximum of 60% yield were obtained without changes in the morphology (Muñoz-Núñez et al. 2022). Then, $NaBH_4$ (10% w/w) were incorporated into the basic solution to prevent depolymerization and degradation of the crystals. This reaction, carried out at 117 °C for 18 h several times, provided

crystalline nano-rod shaped particles with a DA below 20% (Jin et al. 2020b; Jin et al. 2021a). In this study, chitosan preparations were carried out using heterogeneous conditions and the above experimental conditions. In our experiments, a first cycle of deacetylation under strong alkaline solution (NaOH, 40% w/v) at 117 °C overnight was performed in the presence of 10% $NaBH_4$ (w/w) followed by only one more cycle of deacetylation conditions without $NaBH_4$. The determination of the degree of acetylation (DA), listed in Table 1, has been used to conclude on the effectiveness of the reaction (for NMR spectra, see ESI Figures S6 to S8). The impact of the pretreatment was correlated with the obtained DA values after deacetylation of **NCChits** and **IL/DES-pretreated NCChits.** Indeed, chitosans from **untreated NCChits** and **DES-pretreated NCChits** presented DA of 73.2% and 73.6%, respectively after 2 cycles of reaction indicating that DES pretreatment did not enhance the deacetylation efficiency. On the contrary, after IL-pretreatment, the DA value was of 18.2%.

Table 1. Untreated, pretreated chitin nanocrystals and of the resulting chitosan nanocrystals.

Compound	Yield[a] (%)	DTG[b] (%)	CrI[c] (%)	DA[d] (%)
Commercial Chitin	-	378[e]	75 ± 3.8 [e]	87 ± 4.4 [e]
NCChits	33	384	93 ± 4.7	100 ± 5.0
Untreated partially deacetylated NCChits	67	231, 352	84 ± 4.2	73.2 ± 3.7
DES-pretreated NCChits	65.3	380	91 ± 4.6	-
DES-partially deacetylated NCChits	71.1	240, 370	89 ± 4.5	73.6 ± 3.7
IL-pretreated NCChits	78.6	352	79 ± 4.0	-
IL-NCChitosan	52.0	240	48 ± 2.4	18.2 ± 0.9

(a) Yields of all compounds were determined according to the weight difference of the starting material and the final compound; (b) determined using thermogravimetric analysis under nitrogen atmosphere from 50 to 800 °C following by an isotherm at 800 °C under air for 30 minutes; (c) calculated using XDR diffractograms and the empirical equation described by Fan et al. (Fan et al. 2008a); (d) evaluated by solid-state CP-MAS ^{13}C NMR; (e) (Huet et al. 2020) .

These observations are consistent with the crystallinity indexes of the chitosans and partially deacetylated chitins obtained after 2 cycles of deacetylation reaction (Figure 3-B; see also ESI, Figures S9 and S10): (i) a slight decrease was observed for the partially deacetylated chitins obtained from the **untreated NCChits** and **DES-pretreated NCChits** (84% and 89%, respectively) and (ii) a strong decrease was observed for the one obtained after IL-pretreatment (48%) together with a shift of the maximum peak of intensity to a higher angle (yellow vertical line, Figure 3-B). These results are in accordance with the previous findings (Raut et al. 2016; Zhang et al. 2005). Infrared spectroscopy also confirmed the different impact of each solvent (Figure 3-A; see also ESI, Figures S11 and S12). The IR spectrum of the obtained chitosan after deacetylation reaction of **IL-pretreated NCChits** is presented on Figure 3-A, indicating a change in both morphology and chemical composition. The characteristic bands of the

IL-pretreated NCChits at 1653 cm^{-1}, 1627 cm^{-1} and 1551 cm^{-1} corresponding to the amide I and II disappeared after deacetylation which in turn resulted in development of one large band centered at around 1590 cm^{-1} corresponding to the NH_3^+ groups. On the contrary, the IR spectra obtained after deacetylation reaction of **NCChits** and **DES-pretreated NCChits** (see ESI, Figures S11 and S12) did not show any difference compared to the starting materials suggesting that the reaction was not significantly effective and that only a small part of the *N*-acetyl groups was removed from the surface of the nanocrystals.

Thermogravimetric analyses of all products after deacetylation reaction were performed (Figure 4 and see also ESI, Figures S13 to S15). The DTG max values and their comparison with their corresponding starting materials are found in Table 1. The TGA curve of **IL-NCChitosan** showed two stages of weight loss (Figure 4): the first one occurring before 100°C due to loss of water molecules (10%) and the second one starting at 200°C with a DTG_{max} of 240°C corresponding to the primary degradation of pure chitosan with a weight loss of about 43%. For the products obtained after deacetylation reaction of the **untreated NCChits** and **DES-pretreated NCChits**, three stages of weight loss were observed confirming the low efficiency of the reaction and so the partial removal of the *N*-acetyl groups. A first stage could be observed before 100 °C (4.4% water loss), a second one starting between 150-270 °C (20% and 16% for the untreated and DES-pretreated samples respectively), and a third stage between 275-500 °C (43% and 47% for the untreated and DES-pretreated samples respectively). These observations are in agreement with the data obtained by FTIR and solid state ^{13}C NMR. Previous studies have shown that the DTG_{max} values for crustaceans chitin were around 350 °C and that the thermal stability of chitosan was lower and below 300 °C (Sagheer et al. 2009; Abdou et al. 2008) indicating that the decomposition processes are linked to the *N*-acetyl (GlcNAc) units in chitin and to the amine (GlcN) and *N*-acetyl (GlcNAc) residues in chitosan (Wanjun et al. 2005).

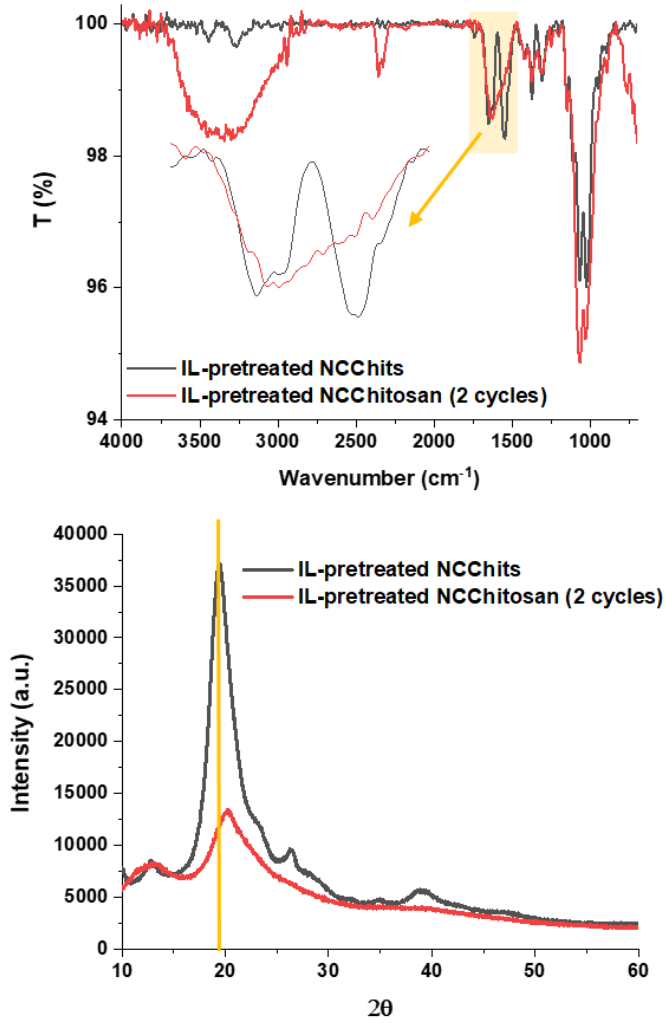

Figure 3. ATR-FTIR spectra of IL-pretreated NCChits (black line) and IL-NCChitosan (red line). Inset: Zoom of the 1750-1450 cm^{-1} range (above) and XRD of IL-pretreated NCChits (black line) and IL-NCChitosan (red line) obtained after 2 cycles of deacetylation reaction (below).

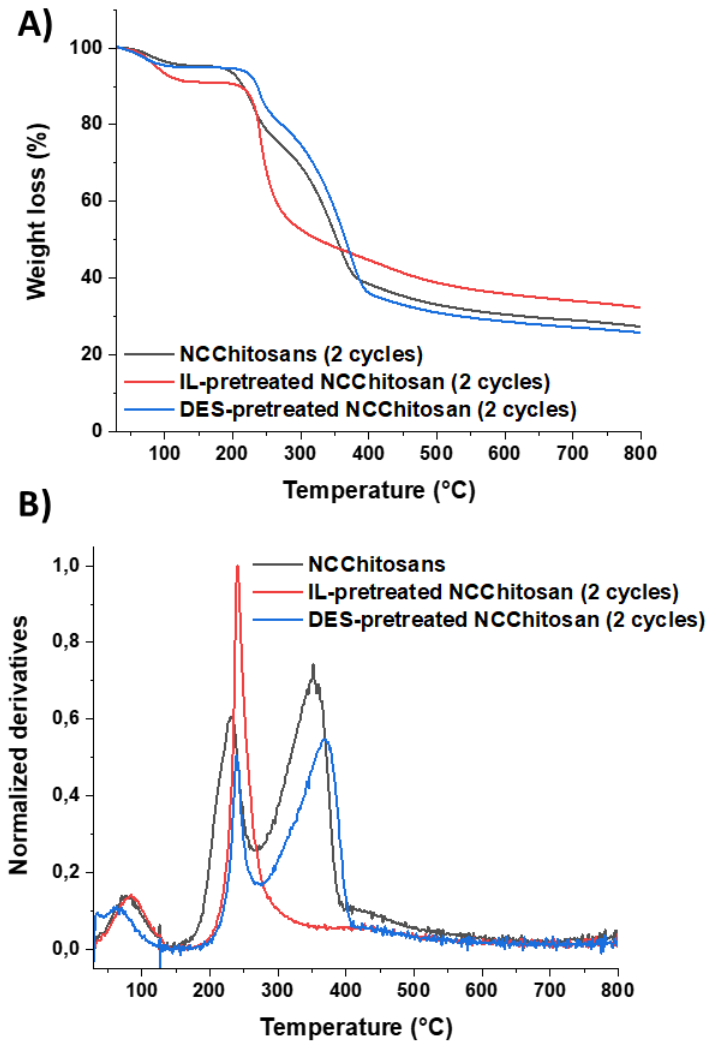

Figure 4. Thermogravimetric (A) and differential thermal analyses (B) of untreated partially deacetylated NCChits (black line), IL-NCChitosan (red line) and DES-partially deacetylated NCChits (blue line) under argon atmosphere from 25 to 800 °C.

3.3. Charge, solubility and morphological studies

Zeta potential measurements of all samples have been performed and compared for the dispersions with a concentration of 1 mg.mL^{-1} in water MQ (pH = 6) at 25 °C . Zeta potential refers to the electrical charges of the surface and is used to quickly investigate the repulsive interactions between colloidal particles and the tendency of agglomeration (Hunter 2013). The measured zeta potential values of the **NCChits** and **IL-pretreated NCChits** were positive with the charge values of 28.06 mV and 37.06 mV, respectively (Table 2). The absolute zeta potential values above +/-20 mV , as obtained here, exhibit colloidal stability (Liu et al. 2019) and have been previously reported in the literature (Fan et al. 2008b; Tsai et al. 2019; Pereira et al. 2014). These positive values resulted from the presence of $–NH_3^+$ groups as reported by Jiang et al. (Jiang et al. 2017). In addition, we previously

reported that IL-pretreatment of chitin did not have any effect on the DA value inducing similar absolute zeta potential values (Huet et al. 2021; Huet et al. 2020a; Huet et al. 2020b). However, the absolute zeta potential value obtained from the dispersion of **DES-pretreated NCChits** under the same conditions gave a negative value of -8.27 mV. This may be due to the presence of negative ions Cl^- in the solution system coming from the CC:LA-DES that could be attracted by the protonated amino groups of the **NCChits**. The zeta-potential values of the **untreated partially deacetylated NCChits** (DA = 73.2%) and **DES-partially deacteylated NCChits** (DA = 73.6%) were of 50.83 mV and 44.92 mV, respectively. This increase may be due to the higher amount of free $-NH_3^+$ groups (Jiang et al. 2017). However, in the case of the highly deacetylated **IL-NCChitosan** (DA = 18.2%), a slight decrease of the zeta-potential value was observed (31.29 mV). The **IL-NCChitosan** tends to aggregate with pH value of MQ water probably due to inter-/intramolecular hydrogen bond formation and the loss of crystallinity (observed visually, Figure 5) (Chang et al. 2015). Thanks to the high content of NH_3^+ groups, **IL-NCChitosan** was fully soluble in acidic media (1%, acetic acid) at a concentration of 10 $mg.mL^{-1}$ and comparable to highly soluble commercially available low molecular weight chitosan at the same concentration. On the contrary, **untreated partially deacetylated NCChits** and **DES-partially deacetylated NCChits** were not soluble but still found to be well dispersed (Figure 5).

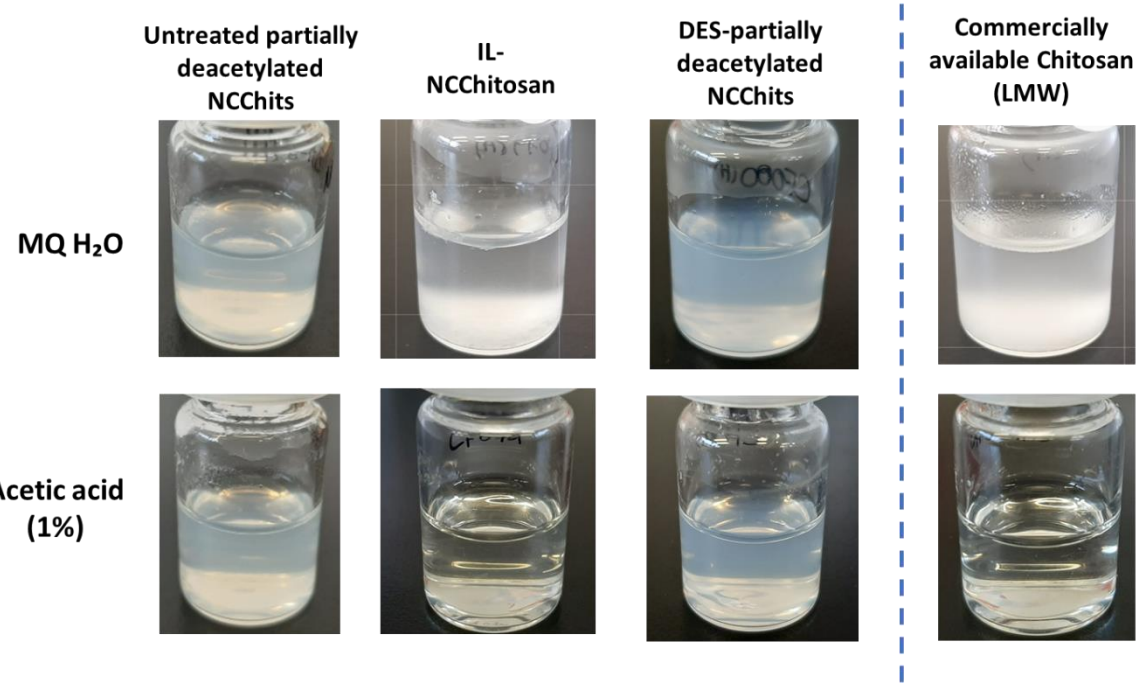

Figure 5. Solubility tests of the obtained NCChitosan and partially deacetylated NCChits synthetized from untreated and IL/DES-pretreated NCChits. Solubility tests of commercially available chitosan (LMW) as a reference. Concentration = 10 $mg.mL^{-1}$ in MQ water or acetic acid (1%).

Table 2. Size distribution and zeta potential of untreated and pretreated chitin nanocrystals and of the resulting NCChitosan and partially deacetylated NCChits.

Compound	Size (% intensity)[a] (nm)	ζ-potential[a] (mV)
NCChits	529.8 (100)	28.06 ± 2.96
Untreated partially deacetylated NCChits	174.0 (100)	50.83 ± 0.87
DES-pretreated NCChits	735.4 (71), 166.5 (28)	-8.27 ± 1.94
DES-partially deacetylated NCChits	640.4 (48.5), 203.6 (51.5)	44.92 ± 1.60
IL-pretreated NCChits	1101.1 (82.4), 247.5 (17.6)	37.06 ± 1.91
IL-NCChitosan	4569.3 (20.1), 683.7 (79.5)	31.29 ± 10.8

(a) Size distribution and zeta-potential values were measured using a ZetaSizer Nano ZS (Malvern, UK). Three measurements were performed for each sample.

The IL/DES-pretreatment of nanocrystals and also the deacetylation reaction could give rise to changes in morphology. The size distribution of **NCChits**, **IL-** and **DES-pretreated NCChits** and the products obtained after deacetylation reaction were first evaluated using dynamic light scattering (DLS) techniques (Table 2) which revealed the polydispersity index (PDI) and the homogeneity of particles. The morphology of all samples was then characterized by TEM and SEM (Figure 6, and see also ESI, Figures S16 to S18).

DLS analyses of **NCChits** and **NCChitosan**/**partially deacetylated NCChits** confirmed the nanoscale dimensions of the particles and the monomodal size distribution with peaks centered at 529.8 nm and 174.0 nm, respectively. Figure 1 shows the TEM image and the length distribution of the obtained **NCChits** displaying an uniform rod-like shape with an average of 153 ± 60 nm in length. The size distribution of the **NCChits** was closely related to the acid hydrolysis time and temperature and our results are similar to those described in the literature (Paillet and Dufresne 2001; Sriupayo et al. 2005; Goodrich and Winter 2007b). The difference in size observed between the two methods may be due to the dispersion concentrations used for the measurements. Indeed, DLS measurements of the **NCChits** were performed at a concentration of 1 $mg.mL^{-1}$ promoting the nanocrystals aggregation, while TEM measurements were performed at lower concentrations (0.1 $mg.mL^{-1}$).

TEM images of **DES-pretreated NCChits** and **DES-partially deacetylated NCChits** confirmed that DES-pretreatment did not affect the morphological structure of the nanocrystals (Figure 6-A and -B, respectively). These observations agree with the results obtained by FTIR spectroscopy and XRD analysis. Bimodal particle size distributions were observed for both samples. Some larger particles that were observed could be the result of an aggregation phenomenon. On the other hand, TEM images of **IL-pretreated NCChits** before and after deacetylation reaction revealed a significant morphological modification leading to nanochitin and nanochitosan sheets.

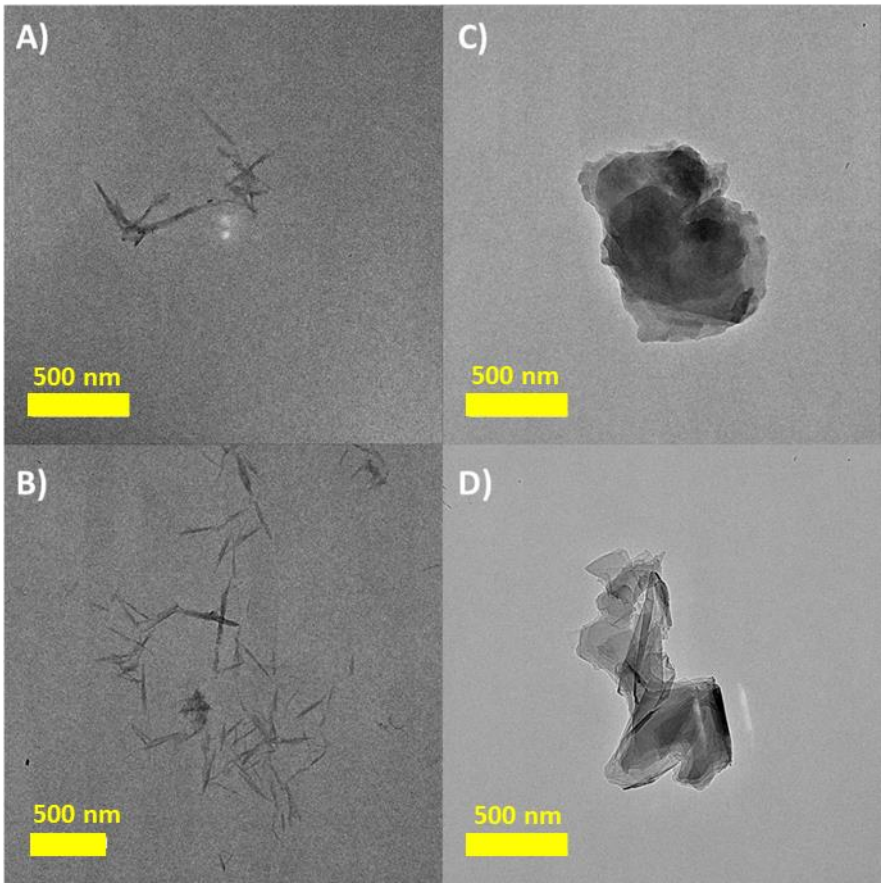

Figure 6. TEM images of the DES-pretreated NCChits (A), DES-partially deacetylated NCChits (B), IL-pretreated NCChits (C) and IL-NCChitosan (D).

3.4. Molecular origins of chitin solvation from *in silico* simulations

The model chitin crystal used for the molecular dynamics simulations consisted of nine 10-mer chains arranged as per experimental crystallographic data (see Computational details); it represents a good tradeoff between realism and computational cost which has already proved successful in previous studies (Uto et al. 2018). It was solvated in IL and DES and simulated for 500 ns at 300 K (room temperature) and 450 K (the *in silico* counterpart to the experimental chitin pretreatment temperature of 353 K – see Material and methods for the justification of this choice).

The simulations in IL at 450 K showed a progressive penetration of [C_2mim] and [OAc] between the chitin chains, causing their separation. This is triggered by the progressive replacement of the chitin interchain hydrogen bonds by new hydrogen bonds formed between [OAc] and the chitin acetamide and hydroxyl groups, which are stronger due to the excess electron density of the charged [OAc] (see ESI, Figure S19). This initially manifests as a fraying at the edges of the chains. At the outer chains, which only interact on one side with the rest of the chitin slab and thus are less strongly bound, the

fraying becomes a cleft, followed by the progressive peeling of the outer chain. The peeling becomes irreversible once it involves at least 4 sugar units and ends with the separation of the outer chain. Some chains were observed to slide along the chitin slab by a few sugar units before diffusing away (Figure 7a). As a result, the rest of the slab restructures to compensate for the lost interactions (Figure 7b-c). Occasionally, the ejected chains were seen to reencounter the main slab and bind to it. Such events were probably overestimated in our simulations because periodic boundary conditions limit the maximum separation distance between molecular entities; however, this does not invalidate the probable experimental existence of this recomplexation mechanism.

A closer look at the distribution of ions in partially peeled structures revealed that while [OAc] is essential in triggering the dissociation process, [C_2mim] is the driving force keeping the peeled chains separated from one another. Not only does [C_2mim] interact favorably with negative partial charges on the sugars due to its overall positive charge; several [C_2mim] molecules can also form bridges spanning chitin chains using CH/π-type hydrogen bonds between the rather acidic methyl hydrogens and the π electron density sandwiching the aromatic ring (Figure 8). Such interactions, which have been shown to be quite strong (Nishio 2011; Li and Zhang 2016) are essential to the efficient propagation of the chain peeling process.

On the other hand, simulating a chitin slab with the CC:LA DES did not result in any major modification of the slab conformation within 500 ns of simulation. This could be due to the conjunction of chloride ions being too small to induce chain separation via purely steric effects, and the inability of the uncharged lactic acid to successfully displace chitin-chitin hydrogen bonds. The good performance of the IL in dissociating chitin nanocrystals thus appears to stem from the coexistence of charges and hydrogen-bonding moieties on the same molecular scaffold.

Unlike at 450 K, simulations at 300 K in either [C_2mim][OAc] or DES did not lead to the peeling of chitin chains, although a limited fraying of the chain ends was observed with [C_2mim][OAc]. This can be ascribed to the high free energy cost of rupturing the hydrogen-bond network between neighboring chitin chains, as well as the limited dissociation of ion pairs and reduced diffusion rates at lower temperatures, which hinder the crucial steps of the aforementioned dissociation mechanism.

These *in silico* results provide a valuable atom-level justification of our experimental findings. The progressive peeling of chains from chitin monocrystals under the combined action of [OAc] and [C2mim] observed in our simulations tends to amorphize the chitin material, resulting in a lower crystallinity index; it also increases the surface of the material that is exposed to chemical attack, explaining the enhanced deacetylation efficiency. On the other hand, chitin nanocrystals exposed to DES in our simulations do not undergo major structural transitions, in line with the experimentally observed retention of both crystallinity index and deacetylation potential. Finally, despite the

difficulties in selecting a simulation temperature which best matches experimental conditions (see Material and methods), the absence of peeling in our room-temperature simulations of IL pretreatment justifies the need for elevated temperatures and long durations for the experimental process.

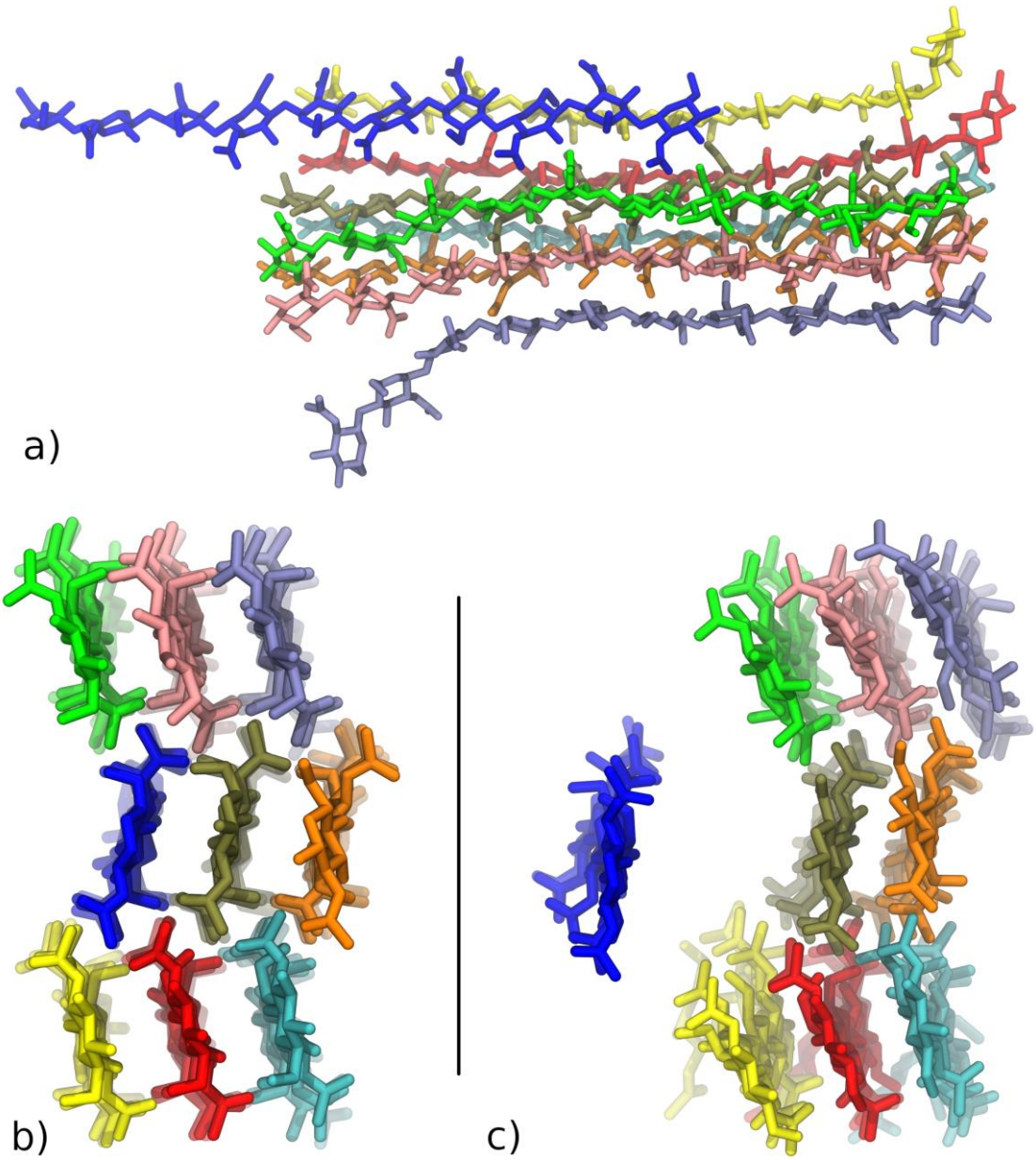

Figure 7. Simulated dissociation of chitin chains in [C_2mim][OAc]. a) Front view of the chains at around 350 ns of simulation time, showing the fraying of terminal groups and the partial dissociation and sliding of outer chains. b-c) Side view of the chains at simulation start (b) and at around 400 ns of simulation (c).

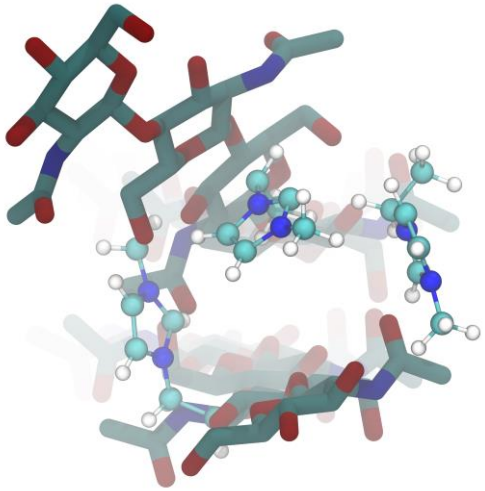

Figure 8. Separation of chitin chains (rods, hydrogen atoms omitted) by bridging IL molecules (balls and sticks). Left: single-IL bridge. Right: two-IL bridge.

4. Conclusions

In this study, we performed an in-depth investigation using both experimental and theoretical approaches on the impact of an ionic liquid 1-ethyl-3-methylimidazolium acetate ([C_2mim][OAc], IL) and a deep eutectic solvent (choline chloride:lactic acid, DES) on extracted chitin nanocrystals. The IL was able to partially break the crystalline structure of the chitin but DES was neither able to break the crystals nor disturb the intra- and intermolecular hydrogen bonds. One of the main properties of [C_2mim][OAc] is its ability to combine the hydrogen-bonding potential of traditional protic solvents with the capacity of ions to form strong electrostatic interactions. Our simulation results show that the coexistence of these two effects is mandatory for the efficient dissociation of chitin chains; they explain the facilitated access of NaOH to the acetamide group, which in turn leads to a higher deacetylation degree for chitin nanocrystals pretreated with IL compared to DES. Moreover, we demonstrate both theoretically and experimentally with SEM images that chitin chains in the crystal can rearrange into sheets. By outlining the relevant molecular-level interactions and mechanisms, these results pave the way toward the production of controlled nanochitosan sheets from chitin nanocrystals.

Acknowledgements

C. F. thanks the doctoral grant of ANID-Chile. A. NVN. thanks the FEDER and the région Hauts-de-France for financial support. The calculations presented in this work were performed using HPC resources from the MATRICS computing platform of Université de Picardie Jules Verne.

Author contributions

C. Ferreira Funes performed the experimental studies. B. Bouvier and C. Cézard were in charge of the computational simulations and wrote the manuscript. A. Jamali performed the TEM images. M. Courty realized the TGA analyses. C. Hadad and C. Fuentealba wrote the manuscript and A. Nguyen Van Nhien supervised and wrote the manuscript.

References

Abdou, E. S., K. S. A. Nagy, and M. Z. Elsabee. 2008. Extraction and characterization of chitin and chitosan from local sources. *Bioresource Technol.* 99 (5):1359-1367.

Agboh, O., and Y. Qin. 1997. Chitin and chitosan fibers. *Polym. Advan. Technol.* 8 (6):355-365.

Abraham, M. J., T. Murtola, R. Schulz, S. Páll, J. C. Smith, B. Hess, and E. Lindahl. 2015. GROMACS: High performance molecular simulations through multi-level parallelism from laptops to supercomputers. *SoftwareX* 1-2:19-25.

Austin, P. R. 1975. Solvents for and purification of chitin: Patent US4062921A.

Azuma, K., S. Ifuku, T. Osaki, Y. Okamoto, and S. Minami. 2014. Preparation and Biomedical Applications of Chitin and Chitosan Nanofibers. *J. Biomed. Nanotechnol.* 10:2891-2920.

Bai, L., L. Liu, M. Esquivel, B. L. Tardy, S. Huan, X. Niu, S. Liu, G. Yang, Y. Fan, and O. J. Rojas. 2022. Nanochitin: Chemistry, Structure, Assembly, and Applications. *Chem. Rev.* 122 (13):11604-11674.

Bisht, M., I. P. E. Macário, M. C. Neves, J. L. Pereira, S. Pandey, R. D. Rogers, J. A. P. Coutinho, and S. P. M. Ventura. 2021. Enhanced Dissolution of Chitin Using Acidic Deep Eutectic Solvents: A Sustainable and Simple Approach to Extract Chitin from Crayfish shell Wastes as Alternative Feedstocks. *ACS Sustain. Chem. Eng.* 9 (48):16073-16081.

Bravo-Osuna, I., C. Vauthier, A. Farabollini, G. F. Palmieri, and G. Ponchel. 2007. Mucoadhesion mechanism of chitosan and thiolated chitosan-poly(isobutyl cyanoacrylate) core-shell nanoparticles. *Biomaterials* 28 (13):2233-2243.

Briscoe, J., A. Marinovic, M. Sevilla, S. Dunn, and M. Titirici. 2015. Biomass-derived carbon quantum dot sensitizers for solid-state nanostructured solar cells. *Angew. Chem. Int. Ed. Engl.* 54 (15):4463-4468.

Chang, S.-H., H.-T. V. Lin, G.-J. Wu, and G. J. Tsai. 2015. pH Effects on solubility, zeta potential, and correlation between antibacterial activity and molecular weight of chitosan. *Carbohydr. Polym.* 134:74-81.

Deringer, V., U. Englert, and R. Dronskowski. 2016. Nature, Strength, and Cooperativity of the Hydrogen-Bonding Network in alpha-Chitin. *Biomacromolecules* 17 (3): 996–1003

Devi, R., and R. Dhamodharan. 2018. Sustainable Process for Separating Chitin and Simultaneous Synthesis of Carbon Nanodots from Shellfish Waste Using 2% Aqueous Urea Solution. *ACS Sustain. Chem. Eng.* 6 (9):11313-11325.

Dhillon, G. S., S. Kaur, S. K. Brar, and M. Verma. 2013. Green synthesis approach: extraction of chitosan from fungus mycelia. *Crit. Rev. Biotechnol.* 33 (4):379-403.

Douard, L., J. Bras, T. Encinas, and M. N. Belgacem. 2021. Natural acidic deep eutectic solvent to obtain cellulose nanocrystals using the design of experience approach. *Carbohydr. Polym.* 252:117136.

Fan, Y., T. Saito, and A. Isogai. 2008a. Chitin Nanocrystals Prepared by TEMPO-Mediated Oxidation of α-Chitin. *Biomacromolecules* 9 (1):192-198.

Fan, I., T. Saito, and A. Isogai. 2008b. Preparation of Chitin Nanofibers from Squid Pen β-Chitin by Simple Mechanical Treatment under Acid Conditions. *Biomacromolecules* 9 (7):1919-1923.

Feng, M., Y. Wang, B. He, X. Chen, and J. Sun. 2022. Chitin-Based Carbon Dots with Tunable Photoluminescence for Fe3+ Detection. *ACS Appl. Nano Mater.* 5 (5):7502-7511.

González, J. A., J. G. Bafico, M. E. Villanueva, S. A. Giorgieri, and G. J. Copello. 2018. Continuous flow adsorption of ciprofloxacin by using a nanostructured chitin/graphene oxide hybrid material. *Carbohydr. Polym.* 188:213-220.

González, J. A., M. F. Mazzobre, M. E. Villanueva, L. E. Díaz, and G. J. Copello. 2014. Chitin hybrid materials reinforced with graphene oxide nanosheets: chemical and mechanical characterisation. *RSC Adv.* 4 (32):16480-16488.

Goodrich, J. D., and W. T. Winter. 2007. Alpha-chitin nanocrystals prepared from shrimp shells and their specific surface area measurement. *Biomacromolecules* 8 (1):252-257.

Goy, R. C., D. d. Britto, and O. B. Assis. 2009. A review of the antimicrobial activity of chitosan. *Polímeros* 19 (3):241-247.

Guo, X., D. Xu, Y. Zhao, H. Gao, X. Shi, J. Cai, H. Deng, Y. Chen, and Y. Du. 2019. Electroassembly of Chitin Nanoparticles to Construct Freestanding Hydrogels and High Porous Aerogels for Wound Healing. *ACS Appl. Mater. Inter.* 11 (38):34766-34776.

Hong, S., Y. Yuan, Q. Yang, P. Zhu, and H. Lian. 2018. Versatile acid base sustainable solvent for fast extraction of various molecular weight chitin from lobster shell. *Carbohydr. Polym.* 201:211-217.

Hong, S., Y. Yuan, K. Zhang, H. Lian, and H. Liimatainen. 2020. Efficient Hydrolysis of Chitin in a Deep Eutectic Solvent Synergism for Production of Chitin Nanocrystals. *Nanomaterials-Basel* 10 (5):869.

Hudson, S. M., and C. Smith. 1998. Polysaccharides: Chitin and Chitosan: Chemistry and Technology of Their Use As Structural Materials. In *Biopolymers from Renewable Resources*, edited by D. L. Kaplan. Berlin, Heidelberg: Springer Berlin Heidelberg, 96-118.

Huet, G., M. Araya-Farias, R. Alayoubi, S. Laclef, B. Bouvier, I. Gosselin, C. Cézard, R. Roulard, M. Courty, C. Hadad, E. Husson, C. Sarazin, and A. Nguyen Van Nhien. 2020a. New biobased-zwitterionic ionic liquids: efficiency and biocompatibility for the development of sustainable biorefinery processes. *Green Chem.* 22 (9):2935-2946.

Huet, G., C. Hadad, E. Husson, S. Laclef, V. Lambertyn, M. Araya Farias, A. Jamali, M. Courty, R. Alayoubi, I. Gosselin, C. Sarazin, and A. N. Van Nhien. 2020b. Straightforward extraction and selective bioconversion of high purity chitin from Bombyx eri larva: Toward an integrated insect biorefinery. *Carbohydr. Polym.* 228:115382.

Huet, G., C. Hadad, J. M. González-Domínguez, M. Courty, A. Jamali, D. Cailleu, and A. N. van Nhien. 2021. IL versus DES: Impact on chitin pretreatment to afford high quality and highly functionalizable chitosan. *Carbohydr. Polym.* 269:118332.

Hunter, R. J. 2013. *Zeta potential in colloid science: principles and applications*. Vol. 2: Academic press.

Ifuku, S., Z. Shervani, and H. Saimoto. 2013. Chitin nanofibers, preparations and applications. *Advances in Nanofibers; Maguire, R., Ed.; IntechOpen: London, UK*:85-101.

Husson, E., C. Hadad, G. Huet, S. Laclef, D. Lesur, V. Lambertyn, A. Jamali, S. Gottis, C. Sarazin, and A. Nguyen Van Nhien. 2017. The effect of room temperature ionic liquids on the selective biocatalytic hydrolysis of chitin via sequential or simultaneous strategies. *Green Chem.* 19 (17):4122-4131.

Jayakumar, R., N. Nwe, S. Tokura, and H. Tamura. 2007. Sulfated chitin and chitosan as novel biomaterials. *Int. J. Biol. Macromol.* 40 (3):175-181.

Jiang, W.-J., M.-L. Tsai, and T. Liu. 2017. Chitin nanofiber as a promising candidate for improved salty taste. *LWT* 75:65-71.

Jin, T., D. Kurdyla, S. Hrapovic, A. C. Leung, S. Régnier, Y. Liu, A. Moores, and E. Lam. 2020. Carboxylated chitosan nanocrystals: a synthetic route and application as superior support for gold-catalyzed reactions. *Biomacromolecules* 21 (6):2236-2245.

Jin, T., T. Liu, S. Jiang, D. Kurdyla, B. A. Klein, V. K. Michaelis, E. Lam, J. Li, and A. Moores. 2021a. Chitosan nanocrystals synthesis via aging and application towards alginate hydrogels for sustainable drug release. *Green Chem.* 23 (17):6527-6537.

Jin, T., T. Liu, E. Lam, and A. Moores. 2021b. Chitin and chitosan on the nanoscale. *Nanoscale Horiz.* 6 (7):505-542.

Jorgensen, W. L., J. Chandrasekhar, J. D. Madura, R. W. Impey, and M. L. Klein. 1983. Comparison of simple potential functions for simulating liquid water. *J. Chem. Phys.* 79 (2):926-935.

Kirschner, K. N., A. B. Yongye, S. M. Tschampel, J. González-Outeiriño, C. R. Daniels, B. L. Foley, and R. J. Woods. 2008. GLYCAM06: A generalizable biomolecular force field. Carbohydrates. *J. Comput. Chem.* 29 (4):622-655.

Lamarque, G., C. Viton, and A. Domard. 2004. Comparative study of the first heterogeneous deacetylation of α-and β-chitins in a multistep process. *Biomacromolecules* 5 (3):992-1001.

Li, J., and R.-Q. Zhang. 2016. Strong orbital interaction in a weak CH-π hydrogen bonding system. *Sci. Rep.* 6 (1):22304.

Li, Z., C. Liu, S. Hong, H. Lian, C. Mei, J. Lee, Q. Wu, M. A. Hubbe, and M.-C. Li. 2022. Recent advances in extraction and processing of chitin using deep eutectic solvents. *Chem. Eng. J.* 446:136953.

Liu, S., Y. Chen, C. Liu, L. Gan, X. Ma, and J. Huang. 2019. Polydopamine-coated cellulose nanocrystals as an active ingredient in poly(vinyl alcohol) films towards intensifying packaging application potential. *Cellulose* 26 (18):9599-9612.

Lv, S., J. Liu, Q. Zhou, L. Huang, and T. Sun. 2014. Synthesis of Modified Chitosan Superplasticizer by Amidation and Sulfonation and Its Application Performance and Working Mechanism. *Ind. Eng. Chem. Res.* 53 (10):3908-3916.

Ma, G., Y. Liu, J. F. Kennedy, and J. Nie. 2011. Synthesize and properties of photosensitive organic solvent soluble acylated chitosan derivatives (2). *Carbohydr. Polym.* 84 (1):681-685.

Mincea, M., A. Negrulescu, and V. Ostafe. 2012. Preparation, modification, and applications of chitin nanowhiskers: a review. *Rev. Adv. Mater. Sci* 30 (3):225-242.

Muñoz-Núñez, C., M. Fernández-García, and A. Muñoz-Bonilla. 2022. Chitin Nanocrystals: Environmentally Friendly Materials for the Development of Bioactive Films. *Coatings* 12 (2):144.

Nishio, M. 2011. The CH/π hydrogen bond in chemistry. Conformation, supramolecules, optical resolution and interactions involving carbohydrates. *Phys. Chem. Chem. Phys.* 13 (31):13873-13900.

Özel, N., and M. Elibol. 2021. A review on the potential uses of deep eutectic solvents in chitin and chitosan related processes. *Carbohydr. Polym.* 262:117942.

Paillet, M., and A. Dufresne. 2001. Chitin Whisker Reinforced Thermoplastic Nanocomposites. *Macromolecules* 34 (19):6527-6530.

Peniche, C., W. Argüelles-Monal, and F. M. Goycoolea. 2008. Chapter 25 - Chitin and Chitosan: Major Sources, Properties and Applications. In *Monomers, Polymers and Composites from Renewable Resources*, edited by M. N. Belgacem and A. Gandini. Amsterdam: Elsevier, 517-542.

Pereira, A. G. B., E. C. Muniz, and Y.-L. Hsieh. 2014. Chitosan-sheath and chitin-core nanowhiskers. *Carbohydr. Polym.* 107:158-166.

Philippova, O. E., E. V. Korchagina, E. V. Volkov, V. A. Smirnov, A. R. Khokhlov, and M. Rinaudo. 2012. Aggregation of some water-soluble derivatives of chitin in aqueous solutions: Role of the degree of acetylation and effect of hydrogen bond breaker. *Carbohydr. Polym.* 87 (1):687-694.

Phongying, S., S.-i. Aiba, and S. Chirachanchai. 2007. Direct chitosan nanoscaffold formation via chitin whiskers. *Polymer* 48 (1):393-400.

Pighinelli, L., M. Guimarães, C. Becker, G. Zehetmeyer, M. Rasia, D. Corrêa, L. Paz, B. Zannin, M. Kmiec, and M. Tedesco. 2016. Structure and properties of nanocrystalline chitosan. *J. Appl. Biotechnol. Bioeng.* 1 (1):1-8.

Popa-Nita, S., P. Alcouffe, C. Rochas, L. David, and A. Domard. 2010. Continuum of structural organization from chitosan solutions to derived physical forms. *Biomacromolecules* 11 (1):6-12.

Ramos, M. L. P., J. A. González, S. G. Albornoz, C. J. Pérez, M. E. Villanueva, S. A. Giorgieri, and G. J. Copello. 2016. Chitin hydrogel reinforced with TiO2 nanoparticles as an arsenic sorbent. *Chem. Eng. J.* 285:581-587.

Raut, A. V., R. K. Satvekar, S. S. Rohiwal, A. P. Tiwari, A. Gnanamani, S. Pushpavanam, S. G. Nanaware, and S. H. Pawar. 2016. In vitro biocompatibility and antimicrobial activity of chitin monomer obtain from hollow fiber membrane. *Designed Monomers and Polymers* 19 (5):445-455.

Rinaudo, M. 2006. Chitin and chitosan: Properties and applications. *Progr. polym. Sci.* 31 (7):603-632.

Roy, J. C., F. Salaün, S. Giraud, A. Ferri, G. Chen, and J. Guan. 2017. Solubility of chitin: solvents, solution behaviors and their related mechanisms. *Solubility of polysaccharides, Ed. Z. xu, IntechOpen* 3:20-60.

Sagheer, F. A. A., M. A. Al-Sughayer, S. Muslim, and M. Z. Elsabee. 2009. Extraction and characterization of chitin and chitosan from marine sources in Arabian Gulf. *Carbohydr. Polym.* 77 (2):410-419.

Serventi, L., Q. He, J. Huang, A. Mani, and A. J. Subhash. 2021. Advances in the preparations and applications of nanochitins. *Food Hydrocolloids for Health* 1:100036.

Shamshina, J. L. 2019. Chitin in ionic liquids: historical insights into the polymer's dissolution and isolation. A review. *Green Chem.* 21 (15):3974-3993.

Sharma, M., C. Mukesh, D. Mondal, and K. Prasad. 2013. Dissolution of α-chitin in deep eutectic solvents. *RSC Adv.* 3 (39):18149-18155.

Shamsuri, A. A., S. N. A. Md. Jamil, and K. Abdan. 2022. Nanocellulose Extraction Using Ionic Liquids: Syntheses, Processes, and Properties. *Frontiers in Materials* 9, A919918.

Sikorski, P., R. Hori, and M. Wada. 2009. Revisit of alpha-chitin crystal structure using high resolution X-ray diffraction data. *Biomacromolecules* 10 (5):1100-1105.

Sriupayo, J., P. Supaphol, J. Blackwell, and R. Rujiravanit. 2005. Preparation and characterization of α-chitin whisker-reinforced chitosan nanocomposite films with or without heat treatment. *Carbohydr. Polym.* 62 (2):130-136.

Sun, C., Z. Wang, L. Chen, and F. Li. 2020. Fabrication of robust and compressive chitin and graphene oxide sponges for removal of microplastics with different functional groups. *Chem. Eng. J.* 393:124796.

Tsai, W.-C., S.-T. Wang, K.-L. B. Chang, and M.-L. Tsai. 2019. Enhancing Saltiness Perception Using Chitin Nanomaterials. *Polymers* 11 (4):719.

Tunjung Seta, F., X. An, and H. Liu. 2021. Solid Acid Hydrolysis for Isolation of Cellulose Nanocrystals and Chitin Nanocrystals – A mini review. *JURNAL SELULOSA* 11:69.

Uto, T., S. Idenoue, K. Yamamoto, and J.-i. Kadokawa. 2018. Understanding dissolution process of chitin crystal in ionic liquids: theoretical study. *Phys. Chem. Chem. Phys.* 20 (31):20669-20677.

Vicente, F. A., B. Bradić, U. Novak, and B. Likozar. 2020. α-Chitin dissolution, N-deacetylation and valorization in deep eutectic solvents. *Biopolymers* 111 (5):e23351.

Wang, J., R. M. Wolf, J. W. Caldwell, P. A. Kollman, and D. A. Case. 2004. Development and testing of a general amber force field. *J. Comput. Chem.* 25 (9):1157-1174.

Wang, X., P. Zhou, X. Lv, and Y. Liang. 2021. Insight into the structure-function relationships of the solubility of chitin/chitosan in natural deep eutectic solvents. *Mater. Today Commun.* 27:102374.

Wanjun, T., W. Cunxin, and C. Donghua. 2005. Kinetic studies on the pyrolysis of chitin and chitosan. *Polym. Degrad. Stabil.* 87 (3):389-394.

Wineinger, H. B., J. L. Shamshina, A. Kelly, C. King, and R. D. Rogers. 2020. A method for determining the uniquely high molecular weight of chitin extracted from raw shrimp shells using ionic iquids. *Green Chem.* 22 (12):3734-3741.

Wu, Y., T. Sasaki, S. Irie, and K. Sakurai. 2008. A novel biomass-ionic liquid platform for the utilization of native chitin. *Polymer* 49 (9):2321-2327.

Yuan, Y., S. Hong, H. Lian, K. Zhang, and H. Liimatainen. 2020. Comparison of acidic deep eutectic solvents in production of chitin nanocrystals. *Carbohydr. Polym.* 236:116095.

Zhang, Y., C. Xue, Y. Xue, R. Gao, and X. Zhang. 2005. Determination of the degree of deacetylation of chitin and chitosan by X-ray powder diffraction. *Carbohydr. Res.* 340 (11):1914-1917.

Zhong, T., M. P. Wolcott, H. Liu, N. Glandon, and J. Wang. 2020. The influence of pre-fibrillation via planetary ball milling on the extraction and properties of chitin nanofibers. *Cellulose* 27 (11):6205-6216.